Neutron scattering and μSR investigations of quasi-one-dimensional magnetism in the spin = 3/2 compound Li_3RuO_4

P. Manuel,[1] D. T. Adroja,[1,*] Per-Anker Lindgard,[2] A. D. Hillier,[1] P. D. Battle,[3] Won-Joon Son,[4] and Myung-Hwan Whangbo[4]

[1]*ISIS Facility, Rutherford Appleton Laboratory, Chilton, Didcot, Oxon, OX11 0QX, United Kingdom*

[2]*Materials Research Division, Risø National Laboratory for Sustainable Energy, DTU, DK-4000 Roskilde, Denmark*

[3]*Inorganic Chemistry Laboratory, Oxford University, South Parks Road, Oxford, OX1 3QR, United Kingdom*

[4]*Department of Chemistry, North Carolina State University, Raleigh, North Carolina 27695-8204, USA*

(Received 25 August 2011; revised manuscript received 5 October 2011; published 21 November 2011)

The $S = 3/2$, quasi-one-dimensional (1D) zig-zag chain Heisenberg antiferromagnet Li_3RuO_4 has been investigated using heat capacity, inelastic neutron scattering, neutron diffraction, and μSR measurements on a powder sample. Our neutron diffraction and μSR studies confirm a long-range ordering of the magnetic moments on the Ru^{5+} cations below 40 K. The magnetic excitations were measured at various temperatures above and below the three-dimensional (3D) ordering temperature in order to understand the broad peak observed in the temperature dependence of the magnetic susceptibility. At 5 K we have observed two well-defined magnetic excitations at 5.5 meV and 8.5 meV and a weak low-energy peak near ~2 meV. We interpret the 5.5 meV energy peak as a 1D zone-boundary mode and that at 8.5 meV as arising from a maximum away from the zone boundary in the dispersion curve for spin-wave modes along the chain of Ru^{5+} ions. The weaker peak near 2 meV is thought to arise from a weak interchain coupling. Our data are best reproduced using a model with three intrachain interactions and one weak interchain interaction. The experimental spin-exchange interactions are in good agreement with those calculated for a 1D model by density functional theory (DFT) methods. Furthermore, above T_N we observe strong diffuse scattering at the same Q-position as the 5.5 meV mode, which suggests the presence of short-range magnetic correlations above T_N. We have estimated the correlation length $\xi \sim 2.9$ Å at 50 K, which is close to 2.99 Å, the shortest distance between the Ru^{5+} cations along the zig-zag chain.

DOI: 10.1103/PhysRevB.84.174430 PACS number(s): 75.30.Ds, 78.70.Nx, 75.50.−y, 75.30.Et

I. INTRODUCTION

In the past few decades, 3*d* transition-metal oxide systems such as high-temperature superconducting cuprates, nickelates, and colossal-magnetoresistive manganites have generated a great deal of interest in condensed-matter physics research due to the amazing variety of their ground-state properties and, in particular, the interplay between magnetism and (super)conductivity. Magnetism is much less common in 4*d* transition-metal oxides than in 3*d*-based oxides because both the on-site Stoner and Coulomb parameters are lower, whereas the bandwidths tend to be larger because the more extended nature of 4*d* orbitals relative to their 3*d* counterparts leads to stronger hybridization between the *d* orbitals and the oxygen 2*p* orbitals. In fact, among the 4*d*-oxide systems, only those containing ruthenium exhibit long-range ordered magnetism. Consequently, in recent years, there has been a considerable increase in the interest in ruthenium-based 4*d*-oxide systems, known as ruthenates. These adopt a variety of crystal structures, including perovskite, layered structures, and the three-dimensional (3D) geometrically frustrated pyrochlore. Although still not as well studied as 3*d*-based systems, many Ru^{4+} compounds have now been shown to exhibit very exciting physical properties, including orbital ordering in $La_2Ru_4O_{10}$,[1] possible Haldane gap formation in $Tl_2Ru_2O_7$,[2] unconventional superconductivity in Sr_2RuO_4 ($T_C = 1.5$ K),[3] non-Fermi liquid behavior in $La_4Ru_6O_{19}$,[4] and unusual ferromagnetic ordering in $SrRuO_3$ ($T_C = 165$ K).[5] Furthermore, resistivity and optical studies have shown non-Fermi-liquid behavior in the paramagnetic state of both $SrRuO_3$ and $CaRuO_3$.[5] It is noteworthy that even though $Tl_2Ru_2O_7$ has a crystal structure without any low-dimensional characteristics, the magnetic interactions are mainly one dimensional (1D) due to orbital ordering of the Ru^{4+} ions.

The observation of such a wide range of electronic properties suggests that ruthenates sit on the boundary between magnetic and nonmagnetic ground states and are thus relevant to the study of quantum magnetism. It is important to recognize that the chemistry of ruthenium is not restricted to Ru^{4+}. Mixed-metal oxides containing Ru^{5+} have also been synthesized and many of them have been shown to have an antiferromagnetic (AFM) ground state, for example, Sr_2YRuO_6 ($T_N = 32$ K) and Sr_3LiRuO_6 ($T_N = 90$ K).[6,7] Indeed, the value of ruthenium in the study of exotic magnetism is enhanced by the fact that the element can adopt many oxidation states; Ru^{2+} ($4d^6$, $S = 0$), Ru^{3+} ($4d^5$, $S = 1/2$), Ru^{4+} ($4d^4$, $S = 1$), and Ru^{5+} ($4d^3$, $S = 3/2$), thus allowing the possibility of observing both quantum magnetism (for smaller spin values) and pure classical magnetism (for larger spin values). In this paper, we report a detailed investigation of a Ru^{5+} system that shows low-dimensional magnetic behavior despite having a 3D crystal structure. More specifically, we have studied Li_3RuO_4, a compound which has previously been shown to have interesting structural and magnetic properties.[8,9] It has been reported to crystallize in the monoclinic space group $P2/a$ with the possibility of having a 1D magnetic interaction in a real 3D crystal structure, as observed in $Tl_2Ru_2O_7$. The structure of Li_3RuO_4 can be thought of as being derived from the rock-salt structure. It contains isolated zig-zag chains of edge-sharing RuO_6 octahedra embedded in a matrix of LiO_6 octahedra. Pseudo-close-packed planes formed of Li cations alternate with planes containing a mixture of Li

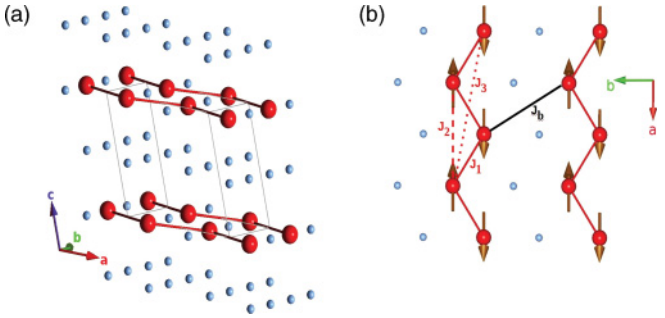

FIG. 1. (Color online) (a) The crystal structure of Li_3RuO_4 showing the presence of 1D zig-zag chain of Ru atoms along a-axis in Li_3RuO_4. For clarity only the metal atoms are shown: Ru-atoms (large red spheres) and Li-atoms (small light-blue spheres). (b) The view of the magnetic structure in the ab-plane with three intrachain interactions along a-axis (J_1, J_2, and J_3) and one interchain interaction along b-axis (J_b). The moments along c-axis are coupled ferromagnetically. Please note that the moment also has a small component along c-axis, which is not shown in Fig. 1(b).

and Ru cations along the body diagonal of the rock-salt subcell. In a mixed Li/Ru plane, the Ru cations form a zig-zag chain interleaved by Li atoms, as is shown in Fig. 1(a). This gives strong intrachain interactions, but weak interchain interactions, resulting in pseudo-1D magnetic interactions between the Ru ions: the nearest-neighbor (NN) Ru-Ru distance in the chain is 2.99 Å. The next-nearest-neighbor (NNN) distance in the chain is 5.10 Å, and the distances between the chains along the b-axis are 4.99 Å and 5.85 Å. The 1D nature of magnetism in Li_3RuO_4 is hinted at by the temperature dependence of the magnetic susceptibility,[8] which exhibits a broad peak at 50 K and strong enhancement in the field-cooled data below 10 K (the origin of the latter is not clear but could be due to small amount of impurity phase).

Recent numerical studies have concentrated on investigations of $S = 3/2$, 2, and 5/2 systems in order to understand the crossover from quantum to classical behavior.[10] However for a real $S = 3/2$ system, the temperature range over which the system shows quantum effects is expected to lie well below T_N. Experimentally, it has been shown, using inelastic neutron scattering, that an $S = 2$ system, $CsCrCl_3$, behaves classically above T_N (16 K).[11] However, recent studies of 1D antiferromagnets have demonstrated the quantum nature of the spin dynamics in $S = 1/2$ and $S = 1$ chains.[12–16] Thus, Li_3RuO_4 with $S = 3/2$ is an ideal system to investigate the crossover from the classical to quantum regime. The present study establishes the existence of an antiferromagnetic ground state for Li_3RuO_4 before going on to characterize the magnetic excitations in Li_3RuO_4, using inelastic neutron scattering to investigate the low-dimensional nature of the magnetism. The study reveals three clear magnetic excitations below the 3D magnetic-ordering temperature, $T_N = 40$ K, and diffuse scattering persisting up to as high as 290 K. We present a classical, theoretical model, which explains the observed magnetic excitations in our powder sample of Li_3RuO_4. The simulation allows us to estimate the three exchange constants, J_1, J_2, and J_3 between Ru spins within a chain (intrachain) and a fourth one, J_b, between the chains (interchain), see Fig. 1(b). We also present an analysis of the temperature dependence of the linewidths and intensities of the excitations and compare them with those observed in other low-dimensional magnetic systems.

II. EXPERIMENTAL DETAILS

The powder sample of Li_3RuO_4 that has been described previously[8] was used in this study. The general materials powder diffraction (GEM) diffractometer at ISIS has high-neutron flux and large detector coverage and hence is ideal for the present study. The sample was cooled to 10 K inside a closed cycle refrigerator (CCR) mounted on the GEM diffractometer at the ISIS pulsed neutron and muon source at the Rutherford Appleton Laboratory, UK, and diffraction patterns were collected at several temperatures between 10 and 70 K with a longer counting time (about 6 hours) for 10 and 70 K. The heat capacity was measured using a physical property measurements system (PPMS), supplied by Quantum Design. Part of the sample was pressed into a pellet and a small piece (∼8 mg) was mounted in the heat capacity rig using a tiny amount of N-grease. The temperature dependence of the heat capacity was measured from 2 to 300 K.

The muon spin rotation (μSR) measurements were carried out in longitudinal geometry using the MuSR spectrometer at ISIS between 2 and 70 K. The powder sample was mounted on a silver (Ag) sample holder and it was cooled down to 2 K in a standard helium cryostat. Any muons implanting on the Ag-sample holder would cause a small time-independent background. We carried out inelastic neutron-scattering experiments on a powder sample (7 g) of Li_3RuO_4 to determine the dynamical scattering function $S(Q, \omega)$ of the $S = 3/2$, 1D-zig-zag chain Heisenberg antiferromagnet. The scattering function $S(Q, \omega)$ was measured between 5 and 300 K on the time-of-flight chopper spectrometer, HET, also at ISIS. The measurements were carried out using incident neutron energies of 18 and 35 meV with instrumental resolutions of 0.69 and 1.19 meV at the elastic position of the 4 m detector bank of HET, respectively. The observed scattering intensity from Li_3RuO_4 was converted into an absolute unit of mb/sr/meV/f.u. by normalizing to the measured intensity from a standard vanadium sample with identical energy settings. The sample was cooled down to 5 K under He-exchange gas in a top-loading CCR.

III. RESULTS AND DISCUSSION

A. Heat capacity measurements

A sharp transition is observed in the heat capacity at 38 K (Fig. 2) with a jump of 12.4 J mol^{-1} K^{-1}, which is indicative of a transition to 3D order at 38 K. No detectable transition at lower temperature is observed. Without the heat-capacity data from a proper phonon-reference compound it was not possible to analyze the heat capacity data below the magnetic-ordering temperature to check whether a gap is present in the magnon spectrum. The observed value of the heat capacity at 300 K is 202 J mol^{-1} K^{-1}, which is in good agreement with that expected from the lattice contribution 199.5 J mol^{-1} K^{-1} for Li_3RuO_4.[17]

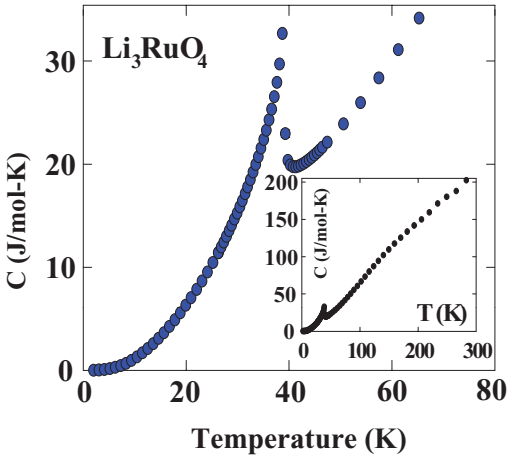

FIG. 2. (Color online) The heat capacity versus temperature of Li_3RuO_4. The inset shows the heat capacity plot up to 300 K.

B. Neutron-diffraction study

Rietveld refinement of the structure of Li_3RuO_4 at 70 K, using data from 5 detector banks (banks 2 to 6, scattering angles $2\theta = 18^\circ$, 35°, 64°, 91°, and 154°) of the GEM diffractometer resulted in a model that is consistent with previously published results[8] [space group $P2/a$ with a = 5.0987(21) Å, $b = 5.847(2)$ Å, $c = 5.0991(19)$ Å, and $\beta = 110.03(1)^\circ$]. As previously, a small amount of Li_2CO_3 (~3%), one of the starting materials for the synthesis, was detected in the sample. Diffraction data from the high-resolution bank (bank-6) are presented along with the calculated pattern in Fig. 3 ($R_f = 3.03$ for the Li_3RuO_4 phase). Data with good counting statistics were also collected at 10 K, the base temperature of the CCR, but, due to time constraints, the temperature evolution of the diffraction pattern between 15 and 40 K was obtained using shorter data collection times. A difference plot (not shown) between the 70 and 10 K data from bank-2 (18°) showed that no extra Bragg peaks appear at low temperature. However, the intensity of some of the nuclear peaks does increase on cooling. The wave vector (Q) dependence of the extra Bragg scattering is typical of a form factor, and its appearance coincides with the disappearance of the paramagnetic scattering at very low Q (see inset of Fig. 4), indicating that it is magnetic in origin and that the system orders with a $k = 0$ structure. A magnetic contribution to the scattering is clearly visible at 4 positions: strong extra scattering is observed at 5.85 Å (0 1 0) and 3.70 Å (0 −1 1, 0 1 1, 1 1 0, and 1 −1 0), while smaller extra contributions are seen around 4.79 Å (001 and 100) and 3.40 Å (−1 −1 1 and −1 1 1). It should be pointed out that a previous low-temperature neutron-diffraction study did not detect any evidence of long-range magnetic ordering[8] due to the magnetic intensity being very weak. The extra flux on GEM compared to that on the instrument used in the previous study made it possible to identify the magnetic Bragg peaks. In order to solve the magnetic structure uniquely, we carried out a symmetry analysis of the Ru atom at the $2e$ position (1/4, 0.8645, 0) with $k = 0$, which reveals that 4 modes are possible according to the irreducible representation of the wave-vector

$$\Gamma mag = \Gamma_1 + \Gamma_2 + 2\Gamma_3 + 2\Gamma_4,$$

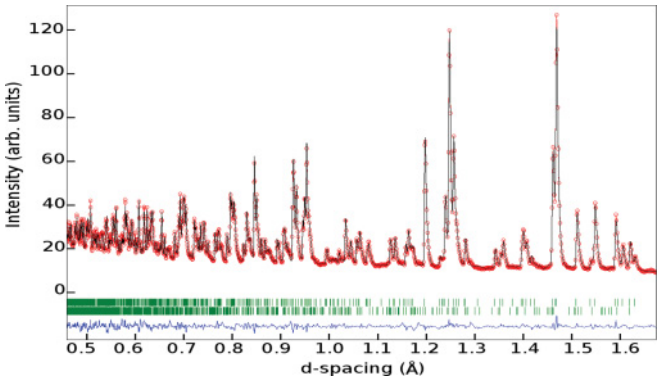

FIG. 3. (Color online) Rietveld refinement of the neutron diffraction data (GEM bank-6) for Li_3RuO_4 at 70 K. The symbols and line represent the experimental and calculated intensities. The two rows of ticks mark the positions of reflections for the main Li_3RuO_4 phase (top) and a small Li_2CO_3 impurity (bottom). The line at the bottom of the plot is the difference between the refinement and the data.

where Γ_1 (Γ_2) corresponds to ferromagnetic (antiferromagnetic) order with the moments aligned along the b-axis. For both of these modes there can be no magnetic contribution to the 010 peak reflection. As this is the strongest contribution observed experimentally, these two modes can clearly be discarded. Γ_3 (Γ_4) corresponds to ferromagnetic (antiferromagnetic) ordering with the atomic magnetic moments confined to the ac-plane. Although it is harder to distinguish between these remaining two modes, using Γ_4 rather than Γ_3 reduces the intensity around 4.79 Å, which is very weak experimentally. Given the antiferromagnetic (AFM) character of the susceptibility and the fact that when using Γ_3 the value of R_{mag} increases, the AFM model is favored. In order to determine unambiguously the moment direction, it would be very useful to obtain single crystals so that further magnetic susceptibility or/and neutron-scattering measurements could be performed. Rietveld analysis of the data collected at 10 K using bank-2 (presented in Fig. 4) and bank-3, using the

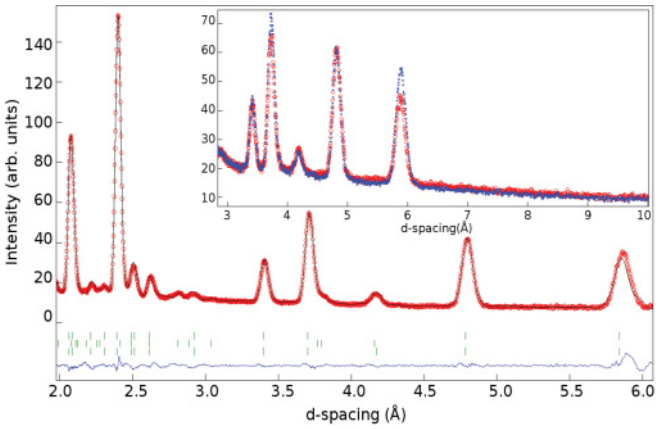

FIG. 4. (Color online) Rietveld refinement (GEM bank-3) for Li_3RuO_4 at 10 K. The conventions are the same as in Fig. 3 with the third row of ticks indicating the position of the calculated magnetic peaks. The inset shows the data at 70 K in big red circles and at 10 K in small blue squares, highlighting the extra intensities on a few Bragg peaks and the loss of paramagnetic scattering at 10 K.

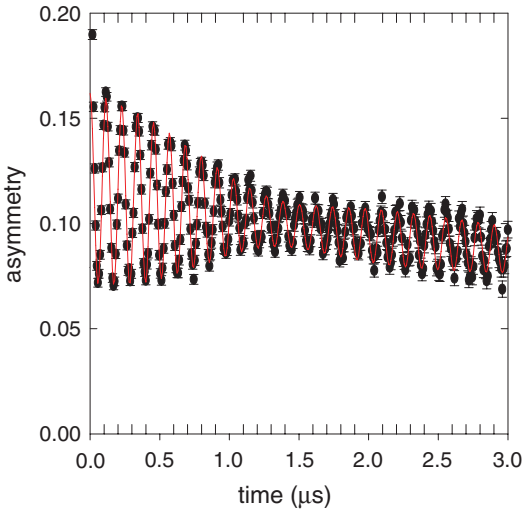

FIG. 5. (Color online) Time evolution of μSR spectrum for Li_3RuO_4 at 1.4 K, focusing at short times. The line is a fit as described in the text.

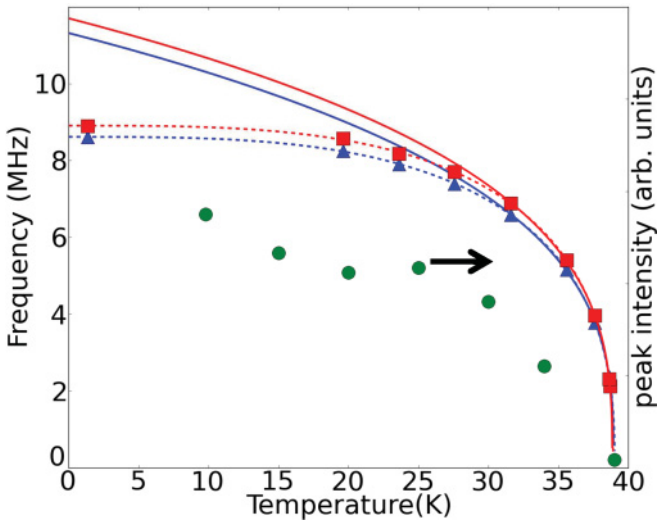

FIG. 6. (Color online) μSR frequencies extracted from the fits to the depolarization spectra as a function of temperature (red squares and blue triangles). The lines are fits to Eq. (2). The solid lines are with $\alpha = 1$, and dotted lines are with α as a variable. The green circles show the extra intensity on the 3.7 Å neutron-diffraction peak (scaled to fit on the same graph).

FullProf program,[18] gave magnetic R-factors of 7.7 and 8.2, respectively; the proposed Γ_4 magnetic structure is presented in Fig. 1(b). Values of the moments are $M_x = 1.93(04)\ \mu_B$, $M_z = -0.19(06)\ \mu_B$, giving a total magnetic moment of $2.00(07)\ \mu_B$, which is close to the values measured previously in other mixed-metal oxides containing the Ru^{5+} cation.[6,7]

C. Zero-field muon spectroscopy study

The MuSR spectrum collected at zero-applied field at 1.5 K is presented in Fig. 5. It is immediately apparent that coherent frequency oscillations characteristic of 3D long-range magnetic ordering are present. Furthermore, the observation of beating indicates that more than one muon frequency is present in the sample. Indeed, the field distribution, determined using a maximum entropy method, reveals the presence of two field components, very close to each other, confirming two muon frequencies. The data are best described by the following equation:

$$A(t) = \sum_{i=1}^{2} \left(a_i \cos(\omega_i t + \varphi) \exp\left(-(\sigma_i t)^2\right) + a_i' \exp(-\lambda_i t)\right) + a_{bkgd}, \quad (1)$$

where ω_i are the frequencies of the oscillations (we used the results from the maximum entropy as starting parameters for each temperature), a_i are the amplitudes of each oscillating component (approximately equal), while a_i' and a_{bkgd} are the lorentzian and background amplitudes. The σ_i are the Gaussian damping of the oscillations, while λ_i are the Lorentzian relaxations. The temperature dependence of the two muon frequencies is presented in Fig. 6, together with that of the 3.7 Å Bragg peak from the neutron diffraction (ND) study. Each muon frequency was fitted to the standard phenomenological equation for temperature evolution of the order parameter[19,20]

$$\omega = \omega_o \left(1 - \left(\frac{T}{T_N}\right)^{\alpha}\right)^{\beta}. \quad (2)$$

We have carried out fits with two methods: (i) with $\alpha = 1$ (fixed) over the temperature range $31 < T/K < 40$ and (ii) with α as a variable over the full temperature range ($10 < T/K < 40$). The extracted parameters from the least squares fit for method-I are as follows: $\alpha = 1$ (fixed) 11.32 and 11.71 MHz for ω_0, 38.99 and 38.86 K for T_N, and 0.32 and 0.31 for β; for method-II, 8.61 and 8.91 MHz for ω_0, 39.02 and 38.91 K for T_N, 0.32 and 0.36 for β, and 3.15 and 3.19 for α. From the high-temperature value of the muon-relaxation rate, it is possible to predict where the muon is located and, as expected, it is close to an oxygen atom. We have used this information together with the magnetic structure determined from our ND data to predict what the magnetic field is likely to be at the muon site, which indeed reveals two sites seeing two very slightly different fields.

D. Inelastic neutron-scattering study

Before discussing the inelastic spectra, it is worth pointing out that, as seen in our ND measurements discussed previously, the HET data with $E_i = 35$ meV (Fig. 7) and 18 meV (Fig. 8) at 5 K also reveal extra magnetic intensity on the Bragg peaks in the elastic channel at $Q = 1.07$ and 1.71 $Å^{-1}$ (covered in 35 meV data, see Fig. 7), as compared with the data for $T \geqslant 50$ K. This further confirms the 3D magnetically ordered ground state of Li_3RuO_4. The Q-integrated data, Fig. 9, show, surprisingly, three well-defined peaks, which we shall call the low-, middle-, and high-energy peak, respectively. They all have a finite energy width even at the lowest temperature, $T = 5$ K. The width and the intensity of the peaks develop quite differently as a function of temperature. The most striking result from the Q-resolved inelastic data is the presence of the two well-resolved spin-wave modes emerging out of the two AFM zone centers with $Q = 1.07$ and 1.71 $Å^{-1}$ at 5 K (see Figs. 7 and 8), corresponding to [0 1 0] and [0 1 1] or [1 1 0]

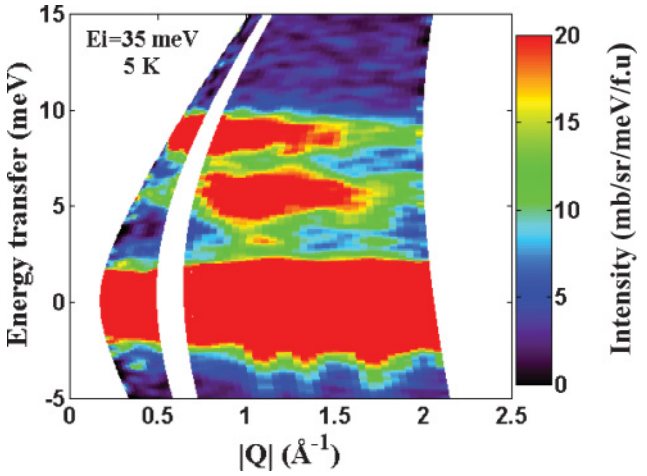

FIG. 7. (Color online) Color contour plot of the scattering intensity, S (Q, ω), plotted as energy transfer versus wave-vector transfer ($|\mathbf{q}| = \mathrm{Q}$) measured using an incident neutron energy of 35 meV at 5 K from Li_3RuO_4.

magnetic Bragg peaks. Figures 8(a)–8(d) show the color contour maps of the scattering intensity, plotted as energy transfer versus momentum transfer, with $E_i = 18$ meV at selected temperatures 5, 40, 50, and 290 K. Figure 8(a) shows two well-defined spin waves modes at 5.5 and 8.5 meV at 5 K in addition to a weak excitation near 2 meV. Interestingly the intensity of the 8.5 meV peak is stronger at lower Q, while the intensity of 5.5 meV peak is very weak at the lowest Q, which is more clear in $E_i = 35$ meV data, see Fig. 7. The energy maximum of the middle- and high-energy modes is nearly Q independent, while that of the low-energy mode near $\sim$2 meV reveals a slight increase in energy with increasing Q: the maximum occurs at 2.9 meV for $Q = 1$–1.5 Å^{-1}. Owing to the instrumental resolution and strong elastic-peak intensities, it is not possible to determine conclusively whether the width of the 2 meV peak changes with Q or not.

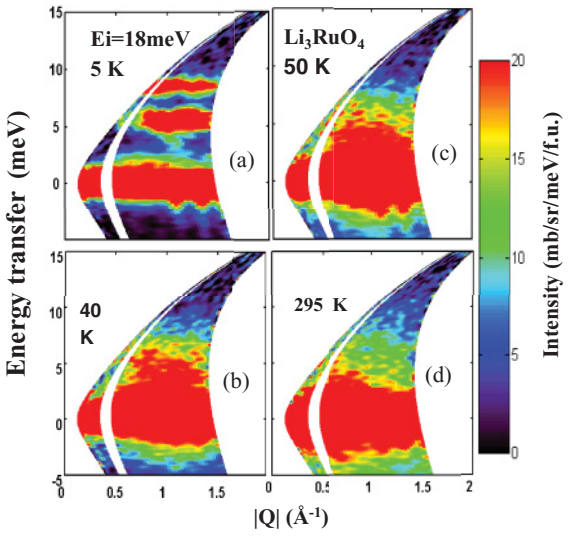

FIG. 8. (Color online) (a–d) Color contour plot of the scattering intensity, S (Q, ω), plotted as energy transfer versus wave-vector transfer ($|\mathbf{q}| = \mathrm{Q}$) measured using an incident neutron energy of 18 meV at various temperatures from Li_3RuO_4.

Figures 9(a)–9(j) show the Q-integrated intensity versus energy cuts from $E_i = 18$ meV data at various temperatures between 5 and 290 K. It is interesting to note from Figs. 9(a)–9(j) that when the temperature is raised from 5 to 36 K, the spin-wave energy of the modes at $\sim$5.5 and 8.5 meV does not change very much. A similar weak-temperature dependence of the spin-wave energies has also been observed for the $S = 1/2$ 1D Heisenberg antiferromagnet, $CuCl_2.2N(C_5D_5)$;[21] it should be noted, however, that for this compound the excitations broaden rapidly. In contrast the intensity of our high-energy mode in Li_3RuO_4 decreases strongly with increasing temperature (see Figs. 8 and 9), and at 40 K (T_N) the high-energy branch has completely disappeared. On the other hand, despite the renormalization of the energy observed near T_N, the middle-energy mode does not disappear above T_N. We have observed a clear inelastic diffuse scattering peak at 50 K, which persists up to 148 K with a nearly temperature-independent position near $\sim$4 meV. Above 148 K, the data could be well fitted with either an inelastic peak or by using only a quasi-elastic peak (Figs. 8 and 9).

The temperature dependence of the intensity of the middle- and high-energy modes between 5 K and T_N of Li_3RuO_4 is interesting. It remains almost constant up to 20 K and then decreases to zero at 40 K for the high-energy mode but increases gradually with temperature up to T_N then decreases slowly above it for the middle-energy mode. Our model subsequently discussed offers an explanation for the different temperature

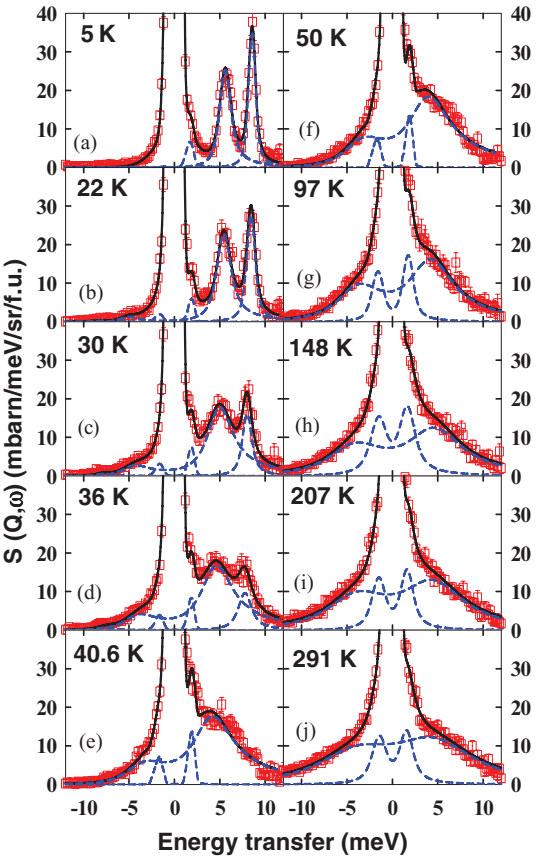

FIG. 9. (Color online) (a–j) Energy transfer versus the Q-integrated intensity of S (Q, ω) at various temperatures. The solid and dotted lines represent the fits (see text).

dependence of the intensity of the middle- and high-energy modes in Li_3RuO_4. The presence of spin waves above T_N in Li_3RuO_4 is reminiscent of other low-dimensional systems, such as $CsVCl_3$, which exhibits 1D magnetism.[22] The spin dynamics of $S = 3/2$ 1D Heisenberg antiferromagnet $CsVCl_3$ have been investigated above and below the 3D magnetic-ordering temperature $T_N = 13.3$ K.[22] This compound also exhibits a well-defined spin-wave mode above T_N, which has been attributed to 1D-type magnetic interactions based on classical spin wave theory.[23] We therefore attribute the presence of the middle-energy mode above T_N in Li_3RuO_4 to the low dimensionality (quasi-1D) of the magnetic interaction between the Ru ions along the zig-zag chain.

IV. SPIN-WAVE ANALYSIS

A. Model and dispersion relation

We present an analysis of the inelastic neutron-scattering data collected on Li_3RuO_4 using two simple spin-wave models. Although the system is almost 1D, we use standard, classical spin-wave theory for 3D, weakly interacting zig-zag linear chains running in the a-direction in the pseudo-close-packed (ab) plane of Li_3RuO_4 [Fig. 1(b)]. We use two sublattices, A and B, for the spin up and down. The lattice vector **b** connects the spins on the same sublattice on adjacent chains, and **a** connects those on the same sublattice along the chain [see Fig. 1(b)]. We assume a simple AFM ground state with the spins in the a-direction (and a-axis taken as quantization axis), see Fig. 1(b). This direction may be stabilized by the presence of a small uniaxial anisotropy; however, the actual direction is not important in the present analysis. Usually, antiferromagnets have two degenerate spin-wave branches, whereas in the presence of a planar anisotropy the branches split up, in particular at low energy. Since there is no evidence for that, we assume no planar anisotropy. We analyze the observed low-temperature spin-wave data with two very simple models. The powder data washes out a number of details in the dispersion relation, hence only a minimal number of interactions can be determined. Consequently we have used interactions in the ab-plane only and have ignored the interactions between the planes, although our spin-dimer analysis (not discussed here) and density functional theory (DFT) calculations[24] indicate that they are not negligible. Both models have three interactions: J_1, J_2, J_3 along the chain and a weak effective interaction between the neighboring chains. It represents the sum of all possible interactions both within the ab-plane and between the planes. For simplicity, we take this to be the in-plane interchain interaction between opposite sublattices [see Fig. 1(b)]. For the first model (model-1), we assume a very small (or no) axial anisotropy and an antiferromagnetic J_b interaction between the chains This model, which is the most natural if the system was a normal 3D antiferromagnet, gives rise to a very small energy gap at $q = 0$. However, if the 1D nature plays a large role there might be a gap. To account for this possibility, we consider as a second case (model-2) a larger axial anisotropy, which effectively can simulate such a gap for the 1D chain-dispersion relation, while we then assume a ferromagnetic J_b coupling between the chains.

The anisotropy and the exchange interaction between the spins are given by the following Hamiltonian

$$\mathrm{H} = -\sum_{\langle ij\rangle} J_{ij}\left(\mathbf{S}_i^A\cdot\mathbf{S}_j^A+\mathbf{S}_i^B\cdot\mathbf{S}_j^B\right)-\sum_{\langle ij\rangle} J'_{ij}\left(\mathbf{S}_i^A\cdot\mathbf{S}_j^B+\mathbf{S}_i^B\cdot\mathbf{S}_j^A\right) - \sum_i\left[D\left(S_i^z\right)^2-P\left(S_i^y\right)^2\right]. \tag{3}$$

Here the first term represents the intrachain interaction (summing over pairs, i.e., J_1, J_2, and J_3) with $\mathbf{S}^A$ and $\mathbf{S}^B$ representing the $S = 3/2$ spin operators on two sublattices. The second term represents the interchain interactions (i.e., J_b), while the third term presents the usual single-ion anisotropy: D is an easy-axial anisotropy and P is a planar anisotropy. For an antiferromagnet the dispersion relations are given by[25]

$$E_q^{\pm} = \left(A_q^2 - C_q^2 - |B_q \pm D_q|^2\right)^{1/2}. \tag{4}$$

We denote the wave vector **q** (as index, q) with the length $|\mathbf{q}| = Q$. The model gives

$$\begin{aligned} A_q &= S(J_0 - J_q + J'_0) + 2D\,(S - 1/2)\,,\\ B_q &= P(S - 1/2),\ C_q = 0,\quad D_q = SJ'_q. \end{aligned} \tag{5}$$

Only in the presence of an anisotropic exchange (dipolar) interaction is C_q different from zero. The Fourier-transformed interaction constants are

$$\begin{aligned} J_q &= 2J_2\cos\left(\mathbf{q}\cdot\mathbf{a}\right),\\ J'_q &= -[(2J_1 + 4J_b\cos(\mathbf{q}\cdot\mathbf{b}))\cos(\mathbf{q}\cdot\mathbf{a}/2) \\ &\quad + 2J_3\cos(3\mathbf{q}\cdot\mathbf{a}/2)]\exp(i\,\mathbf{q}\cdot\mathbf{b}/4). \end{aligned} \tag{6}$$

Here J_1, J_2, J_3 are interactions between neighbors 1–3 along the zig-zag chain, and J_b is the interaction between the chains in the ab-plane (at distance 4.98 Å), as mentioned previously. Since that J_b interaction is very weak, we consider it for simplicity as an effective interaction between linear chains. We neglect a possible interaction between the chains in different planes. Clearly, if there is no planar anisotropy, $P = 0$ and $B_q = 0$, we see from Eq. (4) that the complex part of J'_q does not play a role, and the branches are degenerate with

$$\begin{aligned} E_q = E_q^{\pm} &= S[(J_0 + J'_0 + Ds - J_q - |J'_q|)\\ &\quad\times[(J_0 + J'_0 + Ds - J_q + |J'_q|)]^{1/2}, \end{aligned} \tag{7}$$

where $s = (1 - S/2)$. The **q**-dependent intensity from both branches is then simply proportional to $I_q = A_q/E_q$. In the following powder averaging we neglect the weak dependence $\mathbf{(1 + (\kappa\cdot m)^2)}$ on the relative direction of the unit vectors of the scattering vector $\boldsymbol{\kappa}$ and the sublattice magnetization **m**. The dispersion and the intensity are, of course, strongly dependent on the **q**-direction. As our neutron measurements have been carried out on a powder sample, we have averaged over all **q**-directions to obtain the magnon density of states. The simulated spectra do have peaks where the dispersion is flat. Interestingly three such peaks are observed in the Q-integrated simulated intensity [Figs. 10(a)–10(d)]. This can be accounted for by the simple model using the set of parameters

$$\begin{aligned} \{J_1, J_2, J_3, J_b, D\} = \{&-3.3(1),\ -1.4(1),\ -1.2(1),\\ &-0.010(1),\ 0.0005(5)\}\ \mathrm{meV}. \end{aligned} \tag{8}$$

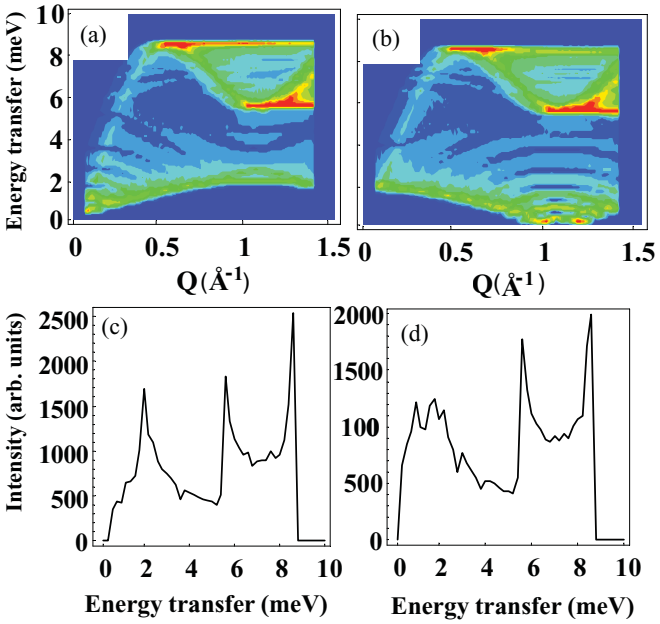

FIG. 10. (Color online) Simulated color contour plot of the powder-averaged scattering plotted as energy transfer versus Q using (a) model-1 with no 1D energy gap at $Q = 0$ and with $D = 0$, and (b) with model-2 having a finite 1D energy gap at $Q = 0$ with $D = 0.05$ meV for Li_3RuO_4 (see text). (c) and (d) represent the corresponding Q-integrated intensity plotted as a function of energy transfer for model-1 and model-2 (see text), respectively.

It was not possible to do a least-squares-fit to the data because the fit involves not only the dispersion relation, but also the intensity, which was measured on a powder sample. However, by exploring the parameter space the error bars are estimated as indicated (referring to the last digit). The parameters J_1, J_2, J_3 are determined by the middle- and high-energy peaks plus the fact that the intensity of the upper peak is the highest. It is not possible to account correctly for all these features by using just J_1, J_2. This is not a strong condition, hence the parameters are correlated—error bars should be understood accordingly. Further, J_b is determined by the lower peak energy at 2 meV. It corresponds to the zone boundary in the b-direction, perpendicular to the chain. J_b is an effective parameter representing the overall interaction between the spin chains. The DFT calculations indicate there may be further small interactions. The anisotropy can be chosen arbitrarily (small) but is useful for stabilizing the ground state. The determined parameters yield a mean-field Néel temperature of $T_N{}^{\rm MF} = 90$ K. As expected in the low-dimensional system, the actual 3D-ordering temperature, $T_N = 40$ K, is much reduced due to fluctuations. Similarly, we can calculate the Curie-Weiss temperature $\Theta_{\rm cal} = -171$ K, which is intermediate between the experimentally determined values (-137 K in Ref. 8, $\Theta_{\rm exp} = -231$ K in Ref. 9). The quasi-1D nature of the magnetic interaction between the Ru spins is apparent along the zig-zag chain, with the strong intrachain NN antiferromagnetic interaction J_1, the weaker J_2, and the weak antiferromagnetic interaction, J_3 plus the hundred-fold weaker AFM interchain interaction J_b [see Fig. 1(b)]. It is interesting to note that these values of the exchange parameters as well as their sign are in excellent agreement with those estimated from DFT calculations using 1D model J_1 (in meV) $= -4.49$, $J_2 = -1.59$, $J_3 = -0.98$, $J_b = 0.0$,[24] indicating the quasi-1D nature of the magnetism of Li_3RuO_4 (see further discussion for details).

The calculated Q-integrated intensity is shown in Fig. 10(a). The middle-energy peak at 5.5 meV corresponds to the zone boundary in the a-direction and the high-energy peak at 8.5 meV to a region near half the zone boundary. This is evident from the density plot of the intensities in the (Q, E_q) plane, Fig. 10(c). One notices the contours of the dispersion relation along the chain (5.5 meV and 8.5 meV peaks) and of that perpendicular to the chain ($\sim$2 meV peak). The powder averaging gives the maximum intensities along three almost Q-independent bands. The high-energy peak has maximum intensity at lower Q, whereas the middle-energy peak picks up at around the zone boundary ($Q = 1.07$ Å^{-1}) and beyond. This is in perfect agreement with the observed intensity behavior in our powder sample of Li_3RuO_4. In this model-1 (for $D = 0$) there is no energy gap at $Q = 0$ for the dispersion of the 1D chain.

Alternatively, we can fit the two higher-energy excitations equally well with a second model-2, which has an energy gap for the linear chain at $q = 0$. This can be done in the simplistic model by choosing a larger $D = 0.05$ meV and a positive interaction between the chains $J_b = 0.008$ meV (and the above values of J_1, J_2, J_3). The results for the (Q, E_q) intensity color contour plot are given in Fig. 10(b), and the Q-integrated intensity of the magnon density of states versus energy transfer is shown in Fig. 10(d). The only change observed in model-2 compared to model-1 is the inverted low-energy ($\sim$2 meV peak) dispersion, but the high-energy response (5.5 meV and 8.5 meV) remains the same in both the models. The parameters determined using the model-2 yield mean-field Néel and Curie temperatures very similar to those calculated using model-1.

The DFT calculations reveal that all the interactions are antiferromagnetic,[24] in support of model-1. The upper-energy part of the dispersion along the chain is already well determined in the present study. Further detailed measurements on a single-crystal sample of Li_3RuO_4 at low energies would be highly desirable to make a clear distinction between the alternative models proposed here as well as to find out whether any other exchange interactions, which are not considered here, are significant. In the analysis we have not considered the full quantum nature of the 1D system. The obtained parameters are therefore effective and may have to be scaled ($\pi/2$ is the scale factor[26] for a linear $S = 1/2$ chain)—but the relative magnitudes should remain the same.

B. Temperature dependence of intensity and width

The temperature dependences of the peak intensity and width of the various modes, discussed subsequently, are both surprising and interesting. The middle- and lower-energy peaks remain intense up to temperature much larger than T_N. We now realize these correspond to zone-boundary excitations. These short-wavelength excitations are known to persist even in the disordered state with strong short-range order.[25] The high-energy peak disappears at T_N, which is consistent with the longer-wavelength nature of that excitation (being from the middle of the zone). Even at the lowest temperatures,

there is a "linewidth" due to the powder averaging, as seen in Figs. 10(c) and 10(d) in comparison with Fig. 9. A more detailed calculation is required in order to account for the detailed behavior of the intensity, energy, and linewidth. However, our simple model-1 accounts for all of the major features observed in this inelastic study of the powder sample of Li_3RuO_4.

Hereafter we present an analysis of the experimentally observed spin-wave linewidth and intensity in Li_3RuO_4 sample. The intrinsic spin-wave linewidth, which is the inverse of the spin-wave lifetime, provides valuable information on the magnon-magnon scattering mechanism. It is directly associated with the relevant damping mechanisms and reflects how the quantized magnons interact with other scattering processes. We have therefore carried out a detailed analysis of spin-wave linewidth using a Lorentzian form of the spectral function convoluted with the instrument resolution (this includes effectively the "linewidth" due to the powder averaging). The instrument-resolution parameters were estimated first by fitting the identical cuts/spectra from monochromatic vanadium runs measured with identical conditions. The following form of $S(Q, \omega)$ was used in our data analysis:

$$S(Q,\omega) = \left(\frac{\omega}{(1-\exp(-\hbar\omega/k_BT)}\right) F^2(Q)\frac{1}{\pi}\sum_i(\chi_i) \times \left(\frac{\Gamma_i}{(\hbar\omega-\hbar\omega_{i0})^2+\Gamma_i^2}+\frac{\Gamma_i}{(\hbar\omega+\hbar\omega_{i0})^2+\Gamma_i^2}\right), \quad (9)$$

where $F^2(Q)$ is the Ru^{5+} form factor taken from Ref. 27, Γ_i is the linewidth, ω_{i0} is the position of the peak, and χ_i is the static susceptibility, which is proportional to the integrated intensity of the peak. We have analyzed both the 35 meV (at 5K) and the 18 meV data at all temperatures between 5 and 300 K. The quality of the fit to 18 meV data can be seen in Fig. 9, and the fit parameters plotted as a function of temperature are shown in Fig. 11. In addition to the middle-energy and high-energy modes, the 18 meV data show a better fit near the elastic tail, when a low-energy peak near 2 meV is added; we attribute the origin of this peak to the low-energy mode arising from the weak interchain interactions, as discussed previously. The data between $T > T_N$ and 291 K were fitted with two methods: (i) a broad inelastic peak near 4 meV and (ii) only a quasielastic peak centered at zero-energy transfer. The data between $T > T_N$ and 148 K can be fitted better with the inelastic peak than with the quasielastic peak, but at 207 and 291 K both of the methods gave equally good fits.

First we discuss the absolute value of the linewidth at 5 K for both the middle-energy (5.5 meV) and high-energy (8.5 meV) modes. Both have larger widths than are accounted for by the powder averaging. The linewidth of the middle-energy mode at 5.5 meV is 0.65 meV, which is 11.8% of the energy of the mode; on the other hand the linewidth of the high-energy mode at 8.5 meV is 0.29 meV, which is 3.4% of the energy of the mode. These values are much smaller than those found in the bilayer manganite, 40% for middle-energy (at 6.2 meV) and 29% for high-energy (at 12 meV) modes, although in both systems the middle-energy mode is much broader than that of high-energy mode.[28] It is to be noted that the width of the high-energy mode near the zone boundary is larger than that of the middle-energy mode in the manganites.[29]

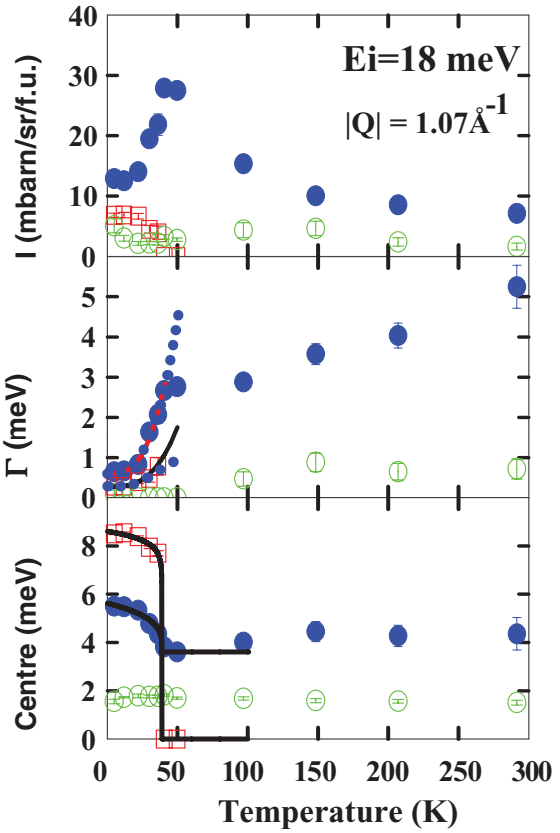

FIG. 11. (Color online) Temperature dependence of the intensity, linewidth, and energy position for the middle-energy and high-energy modes as well as 2 meV peak obtained for the fits (see text).The solid and dotted lines show the fits (see text).

Now we discuss the temperature dependence of the spin-wave linewidth in the AFM-ordered state. We have used two methods to analyze the temperature dependence of the Γ below T_N: (i) power-law behavior, $\Gamma(T) = a_1 \times T^n + b_1$[30] and (ii) thermally activated relaxation rate, $\Gamma(T) = a_2 \times \exp(-\Delta/k_BT)$.[31] The fit to the middle-energy linewidth between 5 and 40 K with all three variables, a_1, n, b_1, was good with $n = 2.9(8)$. However, there was a large error on the estimated value of a_1. Hence, we fixed the value of $n = 3$ and fitted both the data of middle-energy and high-energy modes; the fits are shown by the red solid line in Fig. 11 (middle). It is interesting to compare this exponent value with $n = 3.29$, observed for the Heisenberg antiferromagnet $RbMnF_3$.[30] $n = 3$ is also predicted by the theoretical spin-wave calculations based on the hydrodynamics theory for the four-magnon interaction for some range of energy and temperature by Harris *et al.*[32] Furthermore, the analysis based on the thermally activated relaxation method-II (see dotted line in Fig. 11) also gave an equally good fit for the middle-energy linewidth compared with method-I but not to the high-energy linewidth near T_N. The quality of the fits can be seen in Fig. 11 (middle), dotted line.

There are many sources for linewidth broadening and its temperature dependence: (i) magnon-phonon scattering, (ii) magnon-electron, and (iii) magnon-magnon scattering.

We have not observed any sign of strong phonon peaks, close or overlapping the energy range of the spin-wave branches, hence we rule out the possibility of magnon-phonon interaction. Although we do not have resistivity data on this compound at present, by considering the general behavior of antiferromagnetic transition-metal oxide-systems, we would expect Li_3RuO_4 to behave as an insulator at low temperatures. This also suggests that magnon-electron coupling should be weak. Thus, it is reasonable to assume that magnon-magnon scattering, possibly four-magnon scattering, is playing an important role in the damping of the spin wave in Li_3RuO_4. It should be noted that the four-magnon scattering cross-section is very weak compared to the single-magnon scattering process, hence it would be difficult to observe a direct energy scale and intensity associated with this process in the powder sample. Similar linewidth broadening by four magnon processes has been reported for the antiferromagnet $RbMnF_3$.[30]

Next, we discuss the renormalization of spin-wave energy. We have analyzed the temperature dependence of the energy of both middle-energy (at 5.5 meV) and high-energy (at 8.5 meV) model using the following functional form (i.e., simply renormalized according to the magnetization)

$$E = E_1 + E_0^* \left([T_N - T]/T_N\right)^{\beta}, \tag{10}$$

where β is the critical exponent, E_0 is the magnon energy at $T = 0$, and E_1 is the magnon energy above T_N. The best fit to the high-energy mode gave $T_N = 38.93(1.92)$ K, $\beta_h = 0.044(10)$, $E_{0h} = 8.60\,(06)$ meV, and $E_{1h} = 0$ meV. For fitting the middle-energy mode energy we kept $T_N = 38.93$ K fixed from the previous fit and $E_{1m} = 3.61$ meV fixed from the 50 K data; the best fit gave the value of $\beta_m = 0.29(07)$, $E_{0m} = 2.02\,(08)$ meV. This analysis shows that the two excitations have very different temperature-dependent behavior. Only the renormalization of the middle excitation seems to qualitatively follow the order parameter. We would like to mention here the value of β observed in other low dimensional systems: $\beta = 0.16(0.01)$ has been observed for the 2D spin $S = 5/2$ square-lattice Heisenberg antiferromagnet Rb_2MnF_4,[33] 0.15(0.01) for both the bilayer $K_3Mn_2F_7$ and single-layer K_2MnF_4, 0.138(0.004) for K_2NiF_4,[34] and 0.21(0.01) for bilayer manganites $La_{1.2}Sr_{1.8}Mn_2O_7$.[28]

Finally, we discuss the correlation length and short-range correlations observed above T_N in Li_3RuO_4. The data in Figs. 8 and 9 clearly reveal the presence of short-range diffuse scattering at 50 K near the antiferromagnetic zone center. In order to estimate the correlation length, we have analyzed the difference data, 50–5 K, energy integrated Q-cut, using the following functional form

$$\mathrm{I(Q)} \sim \mathrm{H}/\left((\mathrm{Q} - \mathrm{Q}_0)^2 + \kappa_p^2\right) + \mathrm{bg}. \tag{11}$$

The best fit gives a value of $\kappa_p = 0.36\,(0.08)$, corresponding to a correlation length $\xi = 1/\kappa_p = 2.79(60)$ Å with $H = 1.67(0.85)$, $Q_0 = 1.10(0.02)$, and $bg = 3.5\,(1.5)$. The quality of the fit can be seen in Fig. 12. A different estimate of the correlation length calculated by fitting a Gaussian function to $I(Q)$ gives $\xi \sim 2.0/(2.354 \times \sigma) = 2.97(45)$ Å. These analyses reveal that above T_N we observe the presence of short range correlations only over a distance of the NN Ru-Ru atoms,

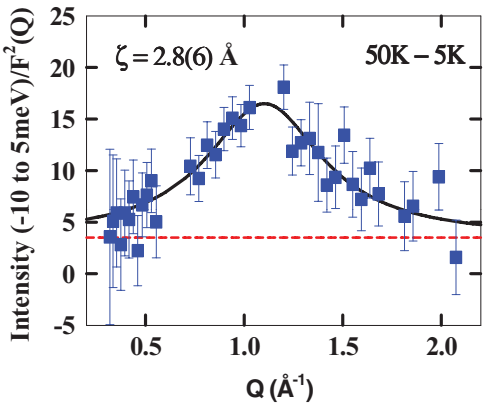

FIG. 12. (Color online) Energy integrated Q-dependence of the temperature difference intensity 50–5 K for $E_i = 35$ meV. The line shows the fit (see text).

which are AFM in nature. The correlation time (τ) of the short-range fluctuations was estimated by fitting a quasi-elastic Lorentzian function, $\tau = \hbar/\Gamma$, to the Q-integrated energy cut at 50 K, giving $\tau = 1.78 \times 10^{-12}$ (s) (and 1.12×10^{-12} (s) at 295 K).

V. DFT ANALYSIS OF SPIN EXCHANGE PARAMETERS

In recent years the energy-mapping analysis based on DFT calculations[35] has been found to give remarkable agreements in determining the relative strengths and the signs of the spin exchange interactions in a variety of transition-metal oxides and hence has provided detailed understanding of their magnetic properties.[36–40] Our DFT evaluation of the spin-exchange interactions of Li_3RuO_4[24] employed the projector augmented wave (PAW) method encoded in the Vienna *ab initio* simulation package (VASP)[36–38] with the generalized gradient approximation (GGA)[39] for the exchange-correlation functional, the DFT plus on-site repulsion U calculations[40] for the Ru 4*d* states, and the crystal structure of Li_3RuO_4 determined at 70 K. The labeling of the interactions used for the calculations is defined in Fig. 1(b). Here we briefly summarize the main outcome of this DFT study relevant for the present spin-wave calculation (for the details of the calculations, see Ref. 24). To check whether or not it is appropriate to use a quasi-1D model for the spin-wave analysis, we evaluated the spin-exchange parameters of Li_3RuO_4 by considering that it is a 3D, 2D, or 1D magnetic system. The values of the relevant spin-exchange interactions estimated with these models are given in Table I. Table I shows that J_b is strongly antiferromagnetic in both 3D and 2D models, and that J_3 is very weakly antiferromagnetic for the 3D model, but very weakly ferromagnetic for the 2D model. Interestingly, for a 1D model, J_3 is strongly antiferromagnetic and is not negligible compared to J_1 and J_2. More interestingly, the magnitudes and signs of J_1, J_2, and J_3 estimated for the 1D model are very close to those estimated from the spin-wave analysis model-1, in strong support of the quasi-1D nature of the interaction in Li_3RuO_4. To further check the 1D nature we simulated the spin-wave dispersion using the spin-exchange parameters of the 3D model shown in Table I. This simulation did not explain the intensities of the 5 and 8 meV modes and did not

TABLE I. The spin-exchange parameters of the 3D, 2D, and 1D spin-lattice models from the GGA + U calculations with U = 3 eV. The last column shows the exchange parameters estimated from the spin-waves analysis, model-1.

	Ru-Ru (Å)	3D	2D	1D	SW-model-1
J_1	2.99	−3.13	−3.22	−4.49	−3.3(1)
J_2	5.10	−1.37	−2.16	−1.59	−1.4(1)
J_3	7.81	−0.30	+0.17	−0.98	−1.2(1)
J_b	4.99	−1.96	−2.51	0.00	−0.010(1)

give the low-energy mode, as observed in our inelastic data. These results strongly support the use of the quasi-1D model for the interpretation of the spin-wave dispersion relations of Li_3RuO_4.

VI. CONCLUSIONS

We have carried out neutron diffraction, μSR, and inelastic neutron-scattering measurements on Li_3RuO_4 to understand the nature of the magnetic ground state in this quasi-1D system. Neutron-diffraction and μSR studies clearly reveal the long-range AFM ordering of the Ru moment with a propagation vector $\mathbf{k} = (0\,0\,0)$ below 40 K. Our inelastic neutron-scattering studies reveal the presence of three spin-wave modes in Li_3RuO_4 below $T_N = 40$ K: a middle-energy mode at 5.5 meV, a high-energy mode at 8.5 meV, and another low-energy mode at 2 meV arising from the interchain interactions between the Ru atoms. Our theoretical spin-wave calculations allow us to estimate the three AFM intrachain interactions [in meV, $J_1 = -3.3(1)$, $J_2 = -1.4(1)$, $J_3 = -1.2(1)$] as well as a much weaker AFM interchain interaction $J_b = -0.010(1)$ meV. The estimated values of the intrachain interactions are in excellent agreement with those calculated using DFT theory for the 1D model, revealing the quasi-1D nature of the magnetism in Li_3RuO_4. Furthermore, above T_N we have observed diffuse scattering arising from the short-range magnetic correlations between the NN Ru ions along the zig-zag chains. We have estimated the correlation length $\xi \approx 2.9$ Å (and correlation time $\tau \approx 1.78 \times 10^{-12}$ sec) at 50 K, which is close to 2.99 Å, the distance between the Ru atoms in the edge-sharing RuO_6 octahedra along the zig-zag chain. We also presented the temperature dependence of the linewidth and the intensities of the inelastic modes. The width of the middle-energy mode at 5.5 meV is higher than that of the high-energy mode at 8.5 meV at lowest temperature, and the difference increases with increasing temperature. Based on the absence of any obvious phonon modes near 5 meV, and the assumption that Li_3RuO_4 exhibits an insulating behavior like other AFM transition-metal oxides, we suggest that the cause of the larger linewidth of the middle-energy mode may be due to magnon-magnon interactions. We expect that the present study will spur further research activity on ruthenates and will prove important in understanding the nature of low-dimensional magnetism in real 3D systems such as Na_3RuO_4.[41]

ACKNOWLEDGMENTS

We would like to acknowledge Radu Coldea, Matthew Stone, Chris Stock, Tapan Chatterji, Alan Tennant, Brian Rainford, Keith McEwen, and J.-G. Park for interesting discussions and Laurent Chapon for his help during the neutron diffraction experiment and interesting discussion on the symmetry analysis. We thank the ISIS facility for providing us with a beam time at ISIS pulsed neutron source. M.-H.W. thanks the financial support from the Office of Basic Energy Sciences, Division of Materials Sciences, US Department of Energy, under Grant No. DE-FG02-86ER45259.

*Corresponding author: devashibhai.adroja@stfc.ac.uk

[1] P. Khalifah, R. Osborn, Q. Huang, H. W. Zandbergen, R. Jin, Y. Liu, D. Mandrus, and R. J. Cava, Science **297**, 2237 (2002).

[2] S. Lee, J.-G. Park, D. T. Adroja, D. Khomskii, S. Streltsov, K. A. McEwen, H. Sakai, K. Yoshimura, V. I. Anisimov, D. Mori, R. Kanno, and R. Ibberson, Nature Materials **5**, 471 (2006).

[3] Y. Maeno, H. Hashimoto, K. Yoshida, S. Nishizaki, T. Fujita, J. G. Bendnorz, and F. Lichtenbereg, Nature **372**, 532 (1994).

[4] P. Khalifah, K. D. Nelson, R. Jin, Z. Q. Mao, Y. Liu, Q. Huang, Y. P. A. Gao, A. P. Ramirez, and R. J. Cava, Nature **411**, 669 (2001).

[5] A. Callaghan, C. W. Moeller, and R. Ward, Inorg. Chem. **5**, 1572 (1966); L. Klein, L. Antognazza, T. H. Geballe, M. R. Beasley, A. Kapitulnik, Physica B **259-261**, 341 (1999).

[6] P. D. Battle and W. J. Macklin, J. Solid State Chem. **52**, 138 (1984).

[7] J. Darriet, F. Grasset, and P. D. Battle, Mater. Res. Bull. **32**, 139 (1997).

[8] A. Alexander, P. D. Battle, J. C. Burley, D. J. Gallon, C. P. Grey, and S. H. Kim, J. Mater. Chem. **13**, 2812 (2003).

[9] M. Soma and H. Sato, J. Phys. Soc. Jpn. **75**, 124802 (2006).

[10] L. Capriotti, R. Vaia, A. Cuccoli, and V. Tognetti, Phys. Rev. B **58**, 273 (1998); L. Capriotti and R. Vaia, *ibid.* **60**, 7299 (1999); N. Hatano and M. Suzuki, J. Phys. Soc. Jpn. **62**, 1346 (1993); S. Yamamoto, Phys. Rev. B **53**, 3364 (1996).

[11] S. Itoh, H. Tanaka, and T. Otomo, J. Phys. Soc. Jpn. **66**, 455 (1997); S. Itoh, H. Tanaka, and M. Bull, *ibid.* **71**, 1148 (2002).

[12] S. R. White and I. Affleck, Phys. Rev. B **54**, 9862 (1996); N. Maeshima, M. Hagiwar, Y. Narumi, K. Kindo, T. C. Kobayashi, and K. Okunishi, J. Phys. Condens. Matter **15**, 3607 (2003).

[13] R. M. Morra, W. J. L. Buyers, R. L. Armstrong, and K. Hirakawa, Phys. Rev. B **38**, 543 (1988).

[14] F. D. M. Haldane, Phys. Lett. **93A**, 464 (1983); Phys. Rev. Lett. **50**, 1153 (1983).

[15] K. Uchinokura, Y. Uchiyama, T. Masuda, Y. Sasago, I. Tsukada, A. Zheludev, T. Hayashi, N. Miura, and P. Böni, Physica B **284–288**, 1641 (2000); A. Lappas, V. Alexandrakis, J. Giapintzakis, V. Pomjakushin, K. Prassides, and A. Schenck, Phys. Rev. B **66**, 14428 (2002); S. M. Rezende and R. M. White, *ibid.* **18**, 2346 (1978).

[16] W. J. L. Buyers, P. M. Morra, R. L. Armstrong, M. J. Hogan, P. Gelrach, and K. Hiraawa, Phys. Rev. Lett. **56**, 3371 (1986); M. Steiner, K. Kakurai, J. K. Kjems, D. Petitgrand, and R. Pynn, J. Appl. Phys. **61**, 3953 (1987).

[17]N. W. Ashcroft and N. D. Mermin, *Solid State Physics* (W. B. Saunders Company, Philadelphia, PA, 1976), p. 427.
[18]J. Rodriguez-Carvajal, Physica B **192**, 55 (1993).
[19]A. J. Steele, T. Lancaster, S. J. Blundell, P. J. Baker, F. L. Pratt, C. Baines, M. M. Conner, H. I. Southerland, J. L. Manson, and J. A. Schlueter, Phys. Rev. B **84**, 064412 (2011).
[20]A. D. Hillier, D. T. Adroja, W. Kockelmann, L. C. Chapon, S. Rayaprol, P. Manuel, H. Michor, and E. V. Sampathkumaran, Phys. Rev. B **83**, 024414 (2011).
[21]Y. Endoh, G. Shirane, R. G. Bergeneau, P. M. Richards, and S. L. Holts, Phys. Rev. Lett. **32**, 170 (1974).
[22]S. Itoh, Y. Endoh, K. Kakurai, H. Tanaka, S. M. Bennington, T. G. Perring, K. Ohoyama, M. J. Harris, K. Nakajima, and C. D. Frost, Phys. Rev. B **59**, 14406 (1999).
[23]S. W. Lovesey, *Theory of Neutron Scattering from Condensed Matter*, Vol. 2 (Clarendon, Oxford, 1984).
[24]Won-Joon Son, P. Manuel, D. T. Adroja, and Myung-Hwan Whangbo, Inorg. Chem. **50**, 9400 (2011).
[25]P. A. Lindgård, A. Kowalska, and P. Laut, J Phys. Chem. Sol. **37**, 1357 (1967).
[26]J. des Cloizeaux and J. J. Pearson, Phys. Rev. **128**, 2131 (1962).
[27]N. G. Parkinson, P. D. Hatton, J. A. K. Howard, C. Ritter, F. Z. Chien, and M. K Wu, J. Mater. Chem. **13**, 1468 (2003).
[28]T. Chatterji, L. P. Regnault, P. Thalmeier, R. van de Kamp, W. Schmidt, A. Hiess, P. Vorderwisch, R. Suryanarayanan, G. Dhalenne, and A. Revcolevschi, J. Alloys Compd. **326**, 15 (2001).
[29]T. G. Perring, D. T. Adroja, G. Chaboussant, G. Aeppli, T. Kimura, and Y. Tokura, Phys. Rev. Lett. **87**, 217201 (2001).
[30]S. M. Rezende and R. M. White, Phys. Rev. B **18**, 2346 (1978).
[31]G. Xu, C. Broholm, D. H. Reich, and M. A. Adams, Phys. Rev. Lett. **84**, 4465 (2000).
[32]A. B. Harris, D. Kumar, B. I. Halperin, and P. C. Hohenberg, Phys. Rev. B **3**, 961 (1971).
[33]R. J. Birgeneau, H. J. Guggenheim, and G. Shirane, Phys. Rev. B **1**, 2211 (1970).
[34]C. M. J. van Uijen, E. Frikkee, and H. W. de Wijnl, Phys. Rev. B **19**, 509 (1979).
[35]P. Hohenberg and W. Kohn, Phys. Rev. **136**, 864 (1964); M. H. Whangbo, H.-J. Koo, and D. J. Dai, Solid State Chem. **176**, 417 (2003).
[36]G. Kresse and J. Hafner, Phys. Rev. B **47**, 558 (1993).
[37]G. Kresse and J. Furthmüller, Comput. Mater. Sci. **6**, 15 (1996).
[38]G. Kresse and J. Furthmüller, Phys. Rev. B **54**, 11169 (1996).
[39]J. P. Perdew, K. Burke, and M. Ernzerhof, Phys. Rev. Lett. **77**, 3865 (1996).
[40]S. L. Dudarev, G. A. Botton, S. Y. Savrasov, C. J. Humphreys, and A. P. Sutton, Phys. Rev. B **57**, 1505 (1998).
[41]K. A. Regan, Q. Huang, and R. J. Cava, J. Solid State Chem. **178**, 2014 (2005); J. T. Haraldsen, M. B. Stone, M. D. Lumsden, T. Barnes, R. Jin, J. W. Taylor, and F. Fernandez-Alonso, J. Phys. Cond. Matter **21**, 506003 (2009).